JMB

Available online at www.sciencedirect.com

SCIENCE DIRECT°

ELSEVIER

Symmetric Primary and Tertiary Structure Mutations within a Symmetric Superfold: A Solution, not a Constraint, to Achieve a Foldable Polypeptide

Stephen R. Brych, Vikash K. Dubey, Ewa Bienkiewicz, Jihun Lee Timothy M. Logan and Michael Blaber*

Kasha Laboratory, Institute of Molecular Biophysics and Department of Chemistry and Biochemistry, Florida State University, Tallahassee, FL 32306-4380, USA

In previous studies designed to increase the primary structure symmetry within the hydrophobic core of human acidic fibroblast growth factor (FGF-1) a combination of five mutations were accommodated, resulting in structure, stability and folding kinetic properties similar to wild-type (despite the symmetric constraint upon the set of core residues). A sixth mutation in the core, involving a highly conserved Met residue at position 67, appeared intolerant to substitution. Structural analysis suggested that the local packing environment of position 67 involved two regions of apparent insertions that distorted the tertiary structure symmetry inherent in the β-trefoil architecture. It was postulated that a symmetric constraint upon the primary structure within the core could only be achieved after these insertions had been deleted (concomitantly increasing the tertiary structure symmetry). The deletion of these insertions is now shown to permit mutation of position 67, thereby increasing the primary structure symmetry relationship within the core. Furthermore, despite the imposed symmetric constraint upon both the primary and tertiary structure, the resulting mutant form of FGF-1 is substantially more stable. The apparent inserted regions are shown to be associated with heparin-binding functionality; however, despite a marked reduction in heparin-binding affinity the mutant form of FGF-1 is surprisingly ~ 70 times more potent in 3T3 fibroblast mitogenic assays. The results support the hypothesis that primary structure symmetry within a symmetric protein superfold represents a possible solution, rather than a constraint, to achieving a foldable polypeptide.

© 2004 Published by Elsevier Ltd.

*Corresponding author

Introduction

Analysis of the structural databank indicates that the overwhelming majority of protein structures can be classified as belonging to one of a very limited number of fundamental protein architectures (currently comprising ten such "super-superfolds").[1,2] These architectures represent a kinetic and thermodynamic solution to the protein folding problem, and their limited number suggests that the evolution of functionality within the proteome is achieved primarily through modification of existing protein architectures, rather than entirely new designs. Experimental and theoretical studies of protein stability and function relationships suggest that novel functionality is typically achieved at the expense of stability (i.e. the "stability/function tradeoff" hypothesis).[3–6] Together, these results suggest that an important property of the ten fundamental superfolds is the ability to accommodate a wide variety of mutations, yet remain stably folded. Thus, the ten fundamental protein architectures likely share a basic property; namely, the potential for substantial thermodynamic stability.

The majority of the fundamental superfolds exhibit some form of tertiary structure symmetry,

---

the postulated result of gene duplication and fusion events during the evolutionary process.[7–13] Despite this tertiary structure symmetry, such proteins may exhibit little if any related primary structure symmetry, indicating that substantial divergence must have occurred following the presumed ancient gene duplication/fusion events. Based upon the stability/function trade-off hypothesis, some fraction of the observed divergence is associated with the emergence of novel functionalities, but at the expense of stability. This leads to the intriguing hypothesis that it may be possible to redesign a protein, belonging to a symmetric superfold, by enforcing a symmetric primary structure constraint, and yet, have the resulting mutant protein increase thermodynamic stability. Such design solutions would have obvious importance in elucidating the process of protein evolution, and also have practical applications in *de novo* protein design.

Human acidic fibroblast growth factor (FGF-1), one of 23 known members of the FGF family, is a member of the β-trefoil superfold and exhibits a characteristic 3-fold tertiary structure symmetry[14–17] (Figure 1). However, as is often the case, this structural symmetry does not extend to the level of the primary structure, which is marginally above random identity when comparing the symmetry-related structural subdomains[18] (Figure 1). In previous reports we have investigated the structural, thermodynamic and kinetic consequences of redesigning the hydrophobic core region with the imposition of a 3-fold symmetric constraint upon

the primary structure.[18,19] These results showed that an alternative core packing group could be identified that exhibited similar kinetic and thermodynamic properties as wild-type. Although no more stable than wild-type it was nonetheless striking that the core could be efficiently repacked despite the 3-fold symmetric constraint upon primary structure. This alternative core did not, however, involve the entire set of 15 core residues. In particular, it was observed that position 67 (a Met residue) appeared intolerant to substitution (e.g. $\Delta\Delta G$ for Met67→Ile was +9.4 kJ/mol, although the other two symmetry-related positions could readily adopt an Ile side-chain).[19] This Met side-chain, which is conserved in 22 of the 23 members of the FGF family, was observed to pack against two adjacent loop structures. Both of these loops, in relationship to their 3-fold symmetry mates, contained insertions within their primary structures (involving residue positions 104–106 and 120–122; Figure 1). These insertions, and their local packing interactions, were postulated as the structural basis for the requirement of the invariant Met at position 67.[19] It was further postulated that if the insertions within these two loops were deleted, that position 67 would exhibit a structural environment similar to its 3-fold symmetry mates, and might therefore accommodate an Ile side-chain.[19] However, it was noted that these loops had functions attributed to them; the loop involving residues 104–106 was a reported low-affinity receptor-binding site, and the loop involving residues 120–122 was part of a heparin-binding site.[15,17,20,21] Thus, while the
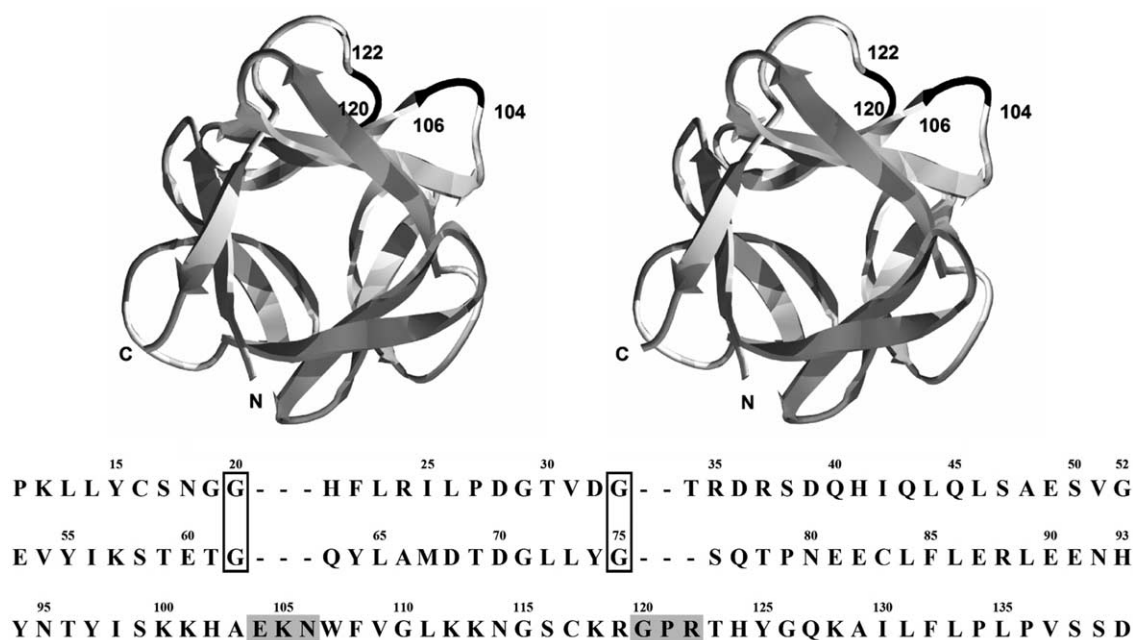
Figure 1. Upper panel: relaxed stereo ribbon diagram of FGF-1 (PDB accession 2AFG) oriented down the 3-fold axis of symmetry, and with the locations of the loop deletions indicated. The amino and carboxyl termini are also indicated. Lower panel: amino acid sequence alignment (using the single-letter code) for the three trefoil subdomains in FGF-1. Shaded residues indicate the locations of the loop deletions in the third domain. The boxed residues indicate Gly amino acids located at the $i+3$ position in local β-turn secondary structure.

Table 1. Nomenclature for mutant forms of FGF-1

Acronym	Mutations
WT[*]	Wild-type (His-tagged)
SYM5	Leu44→Phe/Leu73→Val/Val109→Leu/Leu111→Ile/Cys117→Val
SYM6	Leu44→Phe/Met67→Ile/Leu73→Val/Val109→Leu/Leu111→Ile/Cys117→Val
Δ104–106	Ala103→Gly/ΔGlu104/ΔLys105/ΔAsn106
Δ120–122	Arg119→Gly/ΔGly120/ΔPro121/ΔArg122
ΔΔ	Δ104–106/Δ120–122

proposed loop deletions would increase the structural symmetry, they might simultaneously reduce the activity of specific functionalities.[19]

Here, we describe the biophysical and functional analysis of deletion mutations within the two loops that surround the Met residue at position 67, in combination with an Ile mutation at this position. The results show that the interactions between the loop deletion mutations and position 67 substitution mutation, are highly cooperative and the combination of all three increases the protein stability by a substantial 16.1 kJ/mol. The biophysical characterization of the combination mutant indicates that the heparin-binding affinity has been markedly reduced. Surprisingly, however, this combination mutant exhibits ∼70-fold greater mitogenic potency in comparison to the wild-type protein.

The background form of FGF-1 used for these mutations is the previously reported "SYM5" highly-symmetric core mutant form of FGF-1 (involving five point mutations; Table 1).[19] Thus, the final mutagenized form of FGF-1 resulting from the current study is the most symmetric (at both the tertiary and primary structure level) form of FGF-1 produced to date (involving a total of eight substituted positions combined with six deleted positions). The results therefore provide support for the postulate that a symmetric primary structure within a symmetric protein superfold represents a possible solution to the problem of achieving a highly thermostable folded polypeptide, derivable from gene duplication/fusion events, and useful for subsequent diverse functional adaptive radiation.

Results

Mutant protein production and purification

All mutant proteins, with the exception of the SYM6 mutant were expressed at levels similar to the WT[*] protein (i.e. ∼30–100 mg/l). The SYM6 mutant exhibited a substantially reduced yield, and a tendency to precipitate during purification. The His-tag provides the WT[*] and mutant FGF-1 proteins with nickel-binding affinity, and FGF-1 naturally has a heparin-binding site.[22,23] These two affinity sites were employed in a purification scheme utilizing sequential nickel-NTA and heparin Sepharose affinity chromatography resins.[18] However, mutant forms of FGF-1 involving the Δ120–122 mutation lacked heparin-binding affinity. These mutants were therefore purified by the substitution of gel-filtration chromatography for the heparin Sepharose affinity chromatography. The extinction coefficients used for concentration determination were $E_{280\ nm}$ (0.1%, 1 cm)=1.26 for WT[*] and other mutations not involving deletions or the Leu44Phe point mutation,[24,25] $E_{280\ nm}$ (0.1%, 1 cm)=1.29 for non-deletion mutations involving Leu44Phe, and $E_{280\ nm}$ (0.1%, 1 cm)=1.31 for all deletion mutations (determined by dithionitrobenzoate titration of cysteine residues).

Isothermal equilibrium thermodynamic analysis

Previous studies of the stability and folding of FGF-1 have been performed by monitoring the fluorescence signal of the single buried Trp107 in FGF-1.[18,19,26,27] This Trp in the WT[*] structure is

Table 2. Thermodynamic parameters for WT[*] and mutant FGF-1 proteins as determined by isothermal equilibrium denaturation in guanidine HCl and monitored by CD signal at 227 nm

Protein	ΔG_0 (kJ/mol)	m-value (kJ/mol M)	C_m (M)	$\Delta\Delta G^a$ (kJ/mol)
WT[*]	21.3±0.8	20.1±0.5	1.06±0.01	0.0
SYM5	18.4±0.4	17.5±0.3	1.05±0.01	0.2
SYM5/Δ104–106	25.3±0.9	17.2±0.5	1.47±0.01	−7.6
SYM5/Δ120–122	16.6±0.5	16.6±0.5	1.00±0.02	1.1
SYM5/ΔΔ	34.2±1.2	18.1±0.7	1.89±0.01	−15.9
SYM6[b]	10.4±0.8	19.3±1.9	0.54±0.01	10.2
SYM6/Δ104–106	20.5±0.5	16.9±0.5	1.21±0.01	−2.8
SYM6/Δ120–122	15.7±0.2	20.0±0.2	0.79±0.01	5.4
SYM6/ΔΔ	33.9±0.6	17.7±0.4	1.91±0.02	−16.1

[a] $\Delta\Delta G = (C_{m\ WT*} - C_{m\ mutant})(m_{WT*} + m_{mutant})/2$ as described by Pace.[59] A negative value indicates a more stable mutation in relationship to the wild-type protein. All errors are stated as standard error from multiple data sets.
[b] Previously reported isothermal equilibrium data monitored by fluorescence signal.[19]

somewhat unusual, in that it is more highly quenched in the native state than in the denatured state.[27,28] The Δ120–122 deletion mutant was observed to perturb the fluorescence quenching of Trp107, thus, circular dichroism (CD) spectroscopy was utilized to monitor denaturation for all mutants. The structure of FGF-1 indicates that Trp107 is quenched by Pro121 in the native structure,[17] and the deletion of Pro121 diminishes this quenching. We have previously compared the fluorescence and CD spectroscopic response of FGF-1 to denaturation by GuHCl and shown essentially indistinguishable results for both His-tagged and non-His-tagged forms.[26,27] A tabulation of the mutant thermodynamic data from isothermal equilibrium denaturation, monitored by CD signal, is listed in Table 2. The data in this Table for the SYM6 mutant are from a previously published isothermal equilibrium denaturation study monitored by fluorescence.[19]

Folding and unfolding kinetics

Due to the relatively weak differential CD signal of native and denatured FGF-1, the folding kinetics study required relatively high protein concentrations (>5 mg/ml). While readily soluble in high concentrations of GuHCl, subsequent rapid dilution into the lower GuHCl concentration regime resulted in precipitation for some mutant proteins (i.e. the least stable mutants). Thus, the refolding rate constants were not obtainable below certain denaturant concentrations for these mutants. In addition, the SYM6 mutant typically precipitated during concentration necessary for analysis, and we were unable to obtain any useful kinetic data for this mutant. The SYM6/Δ120–122 mutant is substantially destabilized relative to the WT[*] protein (Table 2) and presents a relatively short "folding arm" in the chevron plot, for this reason there is greater uncertainty associated with the folding kinetics determined for this mutant. Unfolding studies presented no problems associated with precipitation and exhibited single-exponential kinetic properties for each mutant under all denaturant concentrations. Details of the folding and unfolding kinetics of WT[*] FGF-1 in GuHCl denaturant have

been reported.[26] WT[*] FGF-1 exhibits mono-exponential folding behavior over a wide range of denaturant concentrations but deviates to bi-exponential folding behavior (exhibiting a "fast" and "slow" phase) under low denaturant concentrations ($< \sim 0.7$ M).[19,26] The folding kinetics for all mutants, with the notable exception of SYM5/ΔΔ and SYM6/ΔΔ, followed similar folding behavior. The SYM5/ΔΔ and SYM6/ΔΔ, mutants exhibited single-exponential folding behavior under all denaturant concentrations evaluated, and the combination of the loop mutations appears to have eliminated the slow-folding phase observed for WT[*] under low denaturant conditions. The folding and unfolding kinetic data are listed in Table 3. We have previously reported folding and unfolding kinetic data for WT[*] monitored by fluorescence, and note that the data presented here for folding and unfolding, as monitored by CD signal, are in excellent agreement with the prior data.[19,26]

Affinity for sucrose octasulfate determined by isothermal titration calorimetry

FGF-1 mutants that included the Δ120–122 mutation exhibited a substantially reduced heparin-binding affinity to the heparin Sepharose chromatography matrix utilized in purification. To quantify the reduced affinity for heparin (a poly-sulfonated polysaccharide) we determined the affinity for sucrose octasulfate, a structural mimic of a heparin dimer,[29–31] by isothermal titration calorimetry. As part of this evaluation, we compared both WT[*] and the SYM6/ΔΔ mutant, which includes the Δ120–122 mutation. The thermodynamic binding parameters for these proteins are listed in Table 4. We note that our results for the

Table 4. Thermodynamic binding parameters for WT[*] and SYM6/ΔΔ mutant FGF-1 to sucrose octasulfate as determined by isothermal titration calorimetry

| Protein	Stoichi-ometry (n)	K_d (M)	ΔH (kJ/mol)
WT[*]	1.22 ± 0.03	3.5 ± 0.3	-6.7 ± 0.3
SYM6/ΔΔ	1.00 ± 0.09	40.6 ± 2.5	-8.9 ± 1.2

Table 3. Folding and unfolding kinetic parameters for WT[*] and mutant FGF-1 proteins derived from the global (chevron plot) fit using guanidine hydrochloride as the denaturant

Protein	k_f (s^{-1})	m_f (M^{-1})	k_u (1×10^{-3} s^{-1})	m_u (M^{-1})	$\Delta\Delta G_{\ddagger\text{-D}}$ (kJ/mol)[a]	$\Delta\Delta G_{\ddagger\text{-N}}$ (kJ/mol)[a]
WT[*]	3.31	−6.05	0.69	0.47	0	0
SYM5	2.57	−6.44	0.25	0.57	−0.63	−2.51
SYM5/Δ104–106	2.00	−3.70	0.62	0.95	−1.25	−0.25
SYM5/Δ120–122	7.29	−6.44	1.60	0.80	1.96	2.10
SYM5/ΔΔ	40.4	−4.57	0.88	0.66	6.20	0.61
SYM6[b]	–	–	–	–	–	–
SYM6/Δ104–106	30.1	−5.41	3.33	0.94	5.47	3.91
SYM6/Δ120–122	17.3	−9.45	7.95	0.86	4.10	6.07
SYM6/ΔΔ	74.0	−4.40	1.90	0.69	7.70	2.52

[a] Calculated in reference to the WT[*] protein; a positive value indicates a decrease in the associated activation barrier energy.
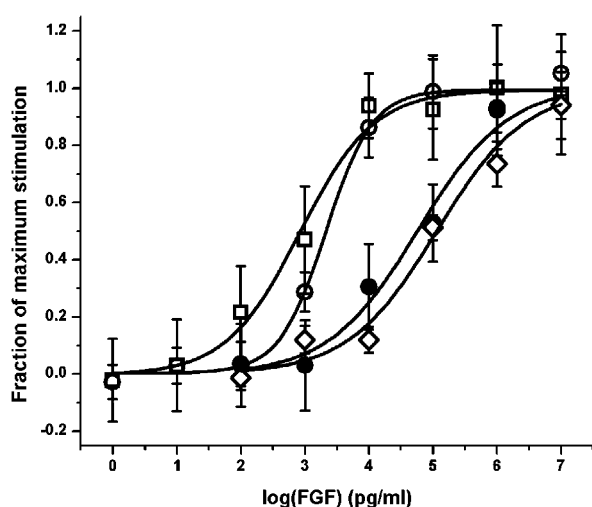[b] Low protein solubility prevents accurate analysis.
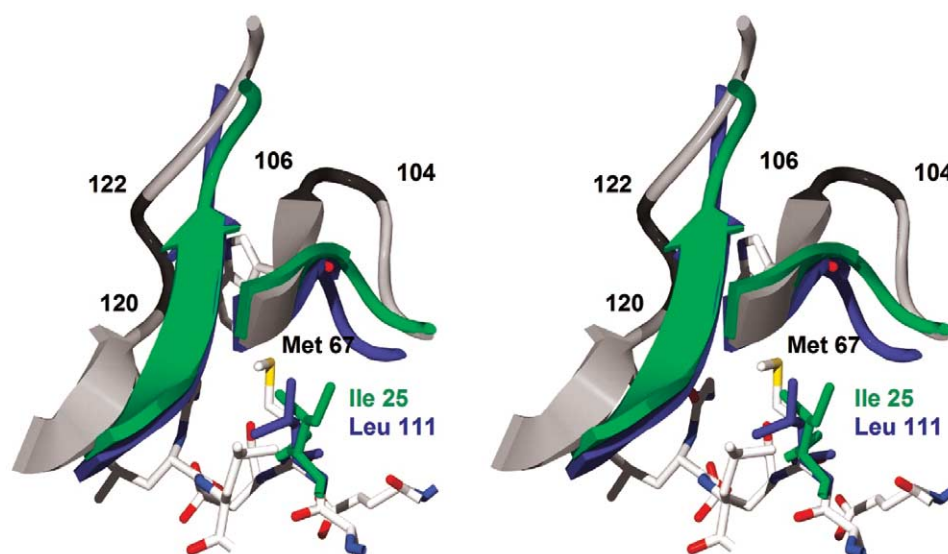
Figure 2. Relaxed stereo image of WT* FGF-1 (PDB accession 1JQZ) in the vicinity of Met67 (CPK colored wireframe representation) with the local loop structures (gray ribbon representation) and indicating the locations of residues 104–106 and 120–122 (deleted regions in the Δ104–106 and Δ120–122 mutations; dark ribbon shading). Overlaid with this are the regions surrounding the symmetry-related positions Ile25 (green color) and Leu111 (blue color) in WT* FGF-1.

titration of WT* FGF-1 with sucrose octasulfate are nearly identical with other published studies.[32]

Mitogenic activity of WT* and mutants of FGF-1

Mitogenic activity towards NIH 3T3 fibroblasts was determined for WT*, SYM5, SYM5/Δ104–106, SYM5/Δ120–122, and SYM6ΔΔ mutants. These mutations are all either more stable or near-WT* in stability, and permit an evaluation of the effects of the loop deletion mutations upon mitogenic activity without concern for false-negatives due to instability effects. The NIH 3T3 fibroblast proliferative

Figure 3. Mitogenic activity assay of WT* and mutant FGF-1 proteins against NIH 3T3 fibroblasts. WT* (●), SYM5/Δ104–106 (◇), SYM5/Δ120–122 (○), and SYM6ΔΔ (□) mutants exhibit EC_{50} values of 60, 115, 2.1, and 0.84 ng/ml, respectively. Standard deviations of the measurements are indicated by the error bars.

activity of WT* FGF-1 yielded an effective concentration for 50% maximal stimulation (EC_{50}) of 60 ng/ml (Figure 3). The SYM5 mutant showed results essentially identical with WT* (data not shown). The SYM5/Δ104–106 mutant exhibited an EC_{50} of 115 ng/ml, or approximately twofold less mitogenic activity in comparison to WT*. Surprisingly, the SYM6ΔΔ mutant exhibited an EC_{50} of 0.84 ng/ml, corresponding to an approximately 70-fold increase in mitogenic activity in comparison to the WT* protein. The SYM5/Δ120–122 mutant exhibited an EC_{50} of 2.1 ng/ml, an approximately 30-fold increase in mitogenic activity compared to WT*, indicating that the increase in mitogenic activity observed for the SYM6ΔΔ mutant was primarily the consequence of the Δ120–122 mutation.

Discussion

In a previous study attempting to constrain the core region of FGF-1 to a symmetric primary structure, a highly conserved Met at position 67 was found to be essential for stability.[19] Since the positions symmetry-related to Met 67 (positions 25 and 111, Figure 1) comprised Ile and Leu side-chains, respectively, the requirement for Met at position 67 was postulated to be due to a unique structural environment surrounding position 67.[19] In particular, it was noted that two loop regions that pack against position 67 contain apparent insertions (i.e. residue positions 104–106 and 120–122) in comparison to the corresponding symmetry-related regions (Figure 2). Furthermore, Met 67 adopts an alternate side-chain χ_1 angle (*trans*) in relationship to either Ile25 or Leu111 (which are both *gauche+*), and consequently orients its side-chain towards the

structural "aneurism" produced by the aforementioned insertions. Analysis of the FGF-1 structure indicated that an Ile or Leu substitution at position 67 (as is observed at the symmetry-related positions 25 and 111, respectively) would result in a substantial cavity within the core region, adjacent to the loop insertions.[19] Thus, it was concluded that simple substitutions were insufficient to achieve a satisfactory alternative symmetric core-packing arrangement, and that modification of the tertiary structure (i.e. deletion of the insertions) was required.

Another previous report, studying the role of Gly residues in stabilizing type I β-turns, investigated the deletion of residue positions 104–106 in FGF-1 and conversion of the local structure into a type I 4 : 6 β-turn.[26] This report identified an essential contribution of a Gly residue at the $i+3$ position within type I β-turns to overall stability. Thus, the 104–106 deletion by itself in the WT* structure resulted in a slight -1.5 kJ/mol increase in stability, but the subsequent Ala103→Gly mutation resulted in a further increase in stability of ~ -6.0 kJ/mol.[26] This study showed that design changes within a protein that result in the formation of a type I β-turn must take into account the nature of the residue at the $i+3$ position within the β-turn (and, in particular, ensure that it is a Gly residue). Using the symmetry-related positions within FGF-1 as a structural guide, the deletion of residue positions 120–122 was similarly postulated to result in the formation of an adjacent β-hairpin turn (involving residue positions 116–119). Residue 119 would correspond to the $i+3$ position in the nascent β-turn. A comparison of the residues symmetry-related to this position (i.e. positions 33 and 75) demonstrated conserved Gly residues in each case (Figure 1). Thus, the 120–122 deletion was combined with an Arg119→Gly mutation in an approach similar to that taken with the 104–106 deletion mutation.[26]

A convenient illustration, representing a series of "double-mutant cycles",[33] of the stability consequences of the combination of each of the two loop deletions and the position 67 substitution mutation is shown in Figure 4. If we start with SYM5 and introduce the Δ104–106 deletion mutant (i.e. the red arrows in Figure 4), it results in a -7.3 kJ/mol increase in stability (essentially identical with the results in the WT* protein[26]). However, if the Δ120–122 deletion mutation is first introduced into SYM5, the Δ104–106 deletion mutant is now observed to increase the stability by -15.4 kJ/mol. Similarly, if position 67 has already been mutated to Ile (to convert SYM5 to SYM6), the Δ104–106 deletion mutant is now observed to increase the stability by -12.1 kJ/mol. Finally, if both the Δ120–122 deletion mutation and the position 67 Ile mutation have already been introduced (i.e. SYM6/Δ120–122 as the background protein), the Δ104–106 deletion mutant is now observed to increase the stability by -21.1 kJ/mol.

When considering the effects of the Δ120–122
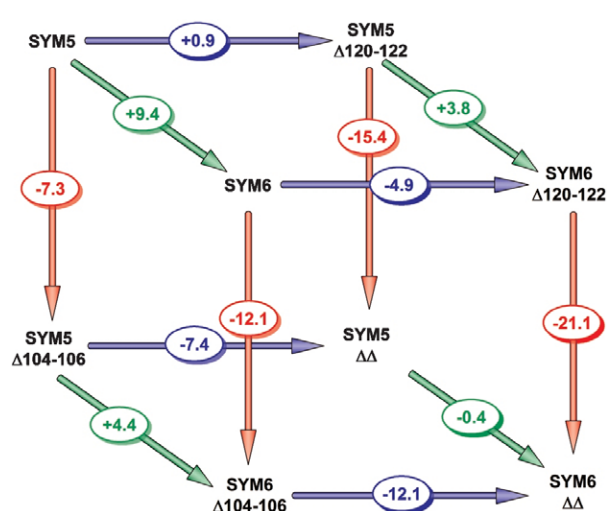
Figure 4. Graphical representation of the effects upon stability for the individual Δ104–106, Δ120–122 and SYM5→SYM6 (i.e. Met67→Ile) mutations when constructed in different background forms of FGF-1. The red arrows indicate the effect of the Δ104–106 mutation, the blue arrows indicate the effect of the Δ120–122 mutation, and the green arrows indicate the effect of the Met67→Ile mutation (i.e. SYM5→SYM6). The ΔΔG values (kJ/mol) for the mutagenic steps are provided, where a negative value indicates that the mutation is stabilizing.

deletion mutation (the blue arrows in Figure 4), unlike the Δ104–106 deletion mutation, the Δ120–122 deletion mutation is not stabilizing when introduced into the SYM5 protein (it exhibits a slight destabilization of $+0.9$ kJ/mol). However, if the Δ104–106 deletion mutation has already been introduced into SYM5, the Δ120–122 deletion mutant is now observed to increase the stability by -7.4 kJ/mol. Similarly, if position 67 has already been mutated to Ile (i.e. SYM6 as the background protein), the Δ120–122 deletion mutant is now observed to increase the stability by -4.9 kJ/mol. Finally, if both the Δ104–106 deletion mutation and the position 67 Ile mutation have already been introduced (i.e. SYM6/Δ104–106 as the background protein), the Δ120–122 deletion mutant is now observed to increase the stability by -12.1 kJ/mol.

When considering the effects of the Met67→Ile mutation (the green arrows in Figure 4), as previously reported, the Met67→Ile mutation destabilizes the SYM5 protein by $+9.4$ kJ/mol.[19] However, if the Δ104–106 deletion mutation has already been introduced into SYM5, the Met67→Ile mutation destabilizes the structure by only $+4.4$ kJ/mol. Similarly, if the Δ120–122 deletion mutation has already been introduced into SYM5, the Met67→Ile mutation destabilizes the structure by only $+3.8$ kJ/mol. Finally, if both the Δ104–106 and Δ120–122 deletion mutations have already been introduced (i.e. SYM5/ΔΔ as the background protein), the Met67→Ile mutation is now observed to actually increase the stability by a modest -0.4 kJ/mol. The effect of combining the two loop

deletions is that the Met residue at position 67 is no longer required for stability (i.e. mutation by Ile is essentially a neutral substitution).

The above analyses indicate a high degree of cooperativity between the two loop deletion mutations and the position 67 substitution. If one considers the SYM5$\Delta\Delta$ protein as a starting frame of reference, the simple sum for the insertion of both loop regions (producing the SYM5 protein) would predict a destabilizing effect of $+22.8$ kJ/mol; however, the resulting effect on stability is only $+15.0$ kJ/mol. Similarly, if one considers a related analysis for the SYM6$\Delta\Delta$ protein, the simple sum of the two loop insertions would predict a destabilizing effect of $+33.2$ kJ/mol when producing the SYM6 protein; however, the actual effect on stability is $+25.3$ kJ/mol. Thus, not only is the Met67 residue helping to mitigate the destabilizing effects of both loop insertions, but also the loops themselves are interacting to minimize destabilization.

A simple sum of the individual mutational effects predicts that, if starting with SYM5, the SYM5$\Delta\Delta$ combination mutant should be destabilizing by $+3.0$ kJ/mol ($-7.3+0.9+9.4$), whereas, the actual combination mutant is -15.1 kJ/mol more stable than the SYM5 protein. Thus, the three structural elements have co-evolved to optimize the stability of their interactions. However, despite these cooperative interactions, the deletion of both loop insertions results in a substantial increase in protein stability of approximately -15 kJ/mol. Thus, regardless of the cooperativity, the protein would be far more stable without these insertions. A reduction in loop length is expected to stabilize the structure due to entropic considerations. The turns at the symmetry-related positions to residues 104–106 are both type I 4 : 6 turns (i.e. four residues within the turn), whereas, the turns at the symmetry-related positions to residues 120–122 are both type I 3 : 5 turns (i.e. three residues within the turn). The expected stability gain from entropic considerations would therefore be approximately -1.5 kJ/mol (for a seven residue to four residue loop conversion) and -2.5 kJ/mol (for a six residue to three residue loop conversion) based upon the loop insertion study by Nagi and Regan.[34] Thus, the approximately -15 kJ/mol increase in stability for the combined loop deletions appears to be primarily enthalpically driven, and represents optimization of non-covalent interactions within the turns and adjacent secondary structure. The stability/function trade-off hypothesis suggests that functional considerations may be associated with the substantial stability penalty associated with adopting the loop insertions.

The lack of affinity for heparin Sepharose by FGF-1 mutants that include the Δ120–122 mutation demonstrates that heparin-binding functionality is contributed by this region. The ITC study of binding to sucrose octasulfate indicates that the binding affinity to this heparin dimer analogue is diminished by an order of magnitude, although it is not completely eliminated (Table 4). Structural and biochemical studies of FGFs identify a key role for heparin in forming a functional signal transduction complex of FGF with its receptor (FGFR).[21,35–40] Thus, it came as a surprise to find that the SYM6$\Delta\Delta$ mutant exhibits an EC$_{50}$ value that is almost two orders of magnitude more potent in comparison to WT* FGF-1 (Figure 3). A comparison with other FGF-1 mutants involving only a single loop deletion indicates that this increase in potency is associated with the Δ120–122 mutation. Why should the diminution of affinity for heparin increase the apparent potency of FGF-1? One possibility is a "free concentration" effect; the majority of FGF-1 added to cells in culture may be sequestered by heparan proteoglycan on the cell surface and may not be directly available for binding to the receptor. However, the Δ120–122 mutation would not be effectively sequestered by heparan proteoglycan (judging from the behavior on heparin Sepharose) and the effective free concentration may therefore be substantially higher than an equivalent concentration of added WT*. The residual heparin-binding affinity (as shown by the ITC data) appears sufficient for formation of an effective FGF/FGFR/heparin signaling complex. Thus, the *in vivo* functionality associated with the loop 120–122 region may be related to sequestering or storage of FGF-1 in heparan proteoglycan on the cell surface, or heparin in the extracellular matrix, rather than relevance to formation of the signaling complex. Such a stored form of FGF-1 could be released during subsequent degradation of the extracellular matrix, as in wound formation or tissue remodeling.[41–44]

The loop 104–106 does not appear to be directly related to heparin binding, and its deletion has little effect upon mitogenic activity (Figure 3). Thus, the loop 104–106 insertion, along with the Met67 residue, may be a mutational response to accommodate the instability associated with the heparin-binding functionality afforded by the insertion of residues 120–122. The SYM6$\Delta\Delta$ mutant exhibits greater mitogenic activity than the sum of the effects of the individual loop deletion mutations exhibited within the SYM5 background. Since cooperative effects upon stability are observed for the loop deletions in combination with the position 67 substitution, this may contribute to the observed non-additive increase in mitogenicity *via* a stability-based mechanism.

The relationship between the folding and unfolding rate constants with denaturant concentration (i.e. chevron plot) for the SYM5 loop mutations is shown in Figure 5. These results illustrate that either loop deletion results in both faster folding and unfolding rates for the mutant FGF-1 protein (in the case of the Δ104–106 deletion the rate of unfolding is increased to a much greater extent than the rate of folding, the net result being an overall destabilization of the protein). This generalized vertical shift of the chevron plot is indicative of a stabilization of the folding transition state ensemble (TSE)[45] (Table 3). Thus, the organization of the local
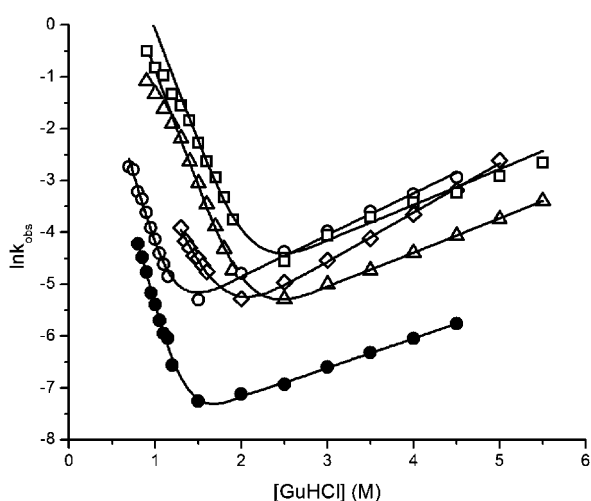
Figure 5. Folding and unfolding rate constants as a function of GuHCl denaturant (i.e. chevron plots) for SYM5 mutants and demonstrating the effects of the loop deletions and position 67 substitution. SYM5 (●), SYM5/Δ104–106 (◇), SYM5/Δ120–122 (○), SYM5ΔΔ (△), and SYM6ΔΔ (□) mutants.

structure involving loops 104–106, 120–122 and Met67 has a key (unfavorable) influence upon the energetics of the TSE in the WT* protein. The observed changes in the energy barrier associated with the TSE (i.e. $\Delta\Delta G_{\ddagger\text{-}D}$ and $\Delta\Delta G_{\ddagger\text{-}N}$, Table 3) highlights the cooperativity between position 67 and the 104–106 and 120–122 loop regions. Furthermore, these results also identify a specific contribution of the Met residue at position 67 in destabilizing the TSE. When comparing the SYM5 loop deletion mutants (containing Met67) with the SYM6 loop deletion mutations (containing Ile67), the Met67 substantially decreases the folding and unfolding rate (Table 3). FGF-1 and other members of the FGF family of proteins are unusual, in that they have no identifiable secretion signal[46,47] and are secreted in an endoplasmic reticulum-independent manner.[48,49] FGF-1 is known to have generally low thermal stability,[27,28] and a partially folded form (i.e. kinetically trapped intermediate) of FGF has been postulated to be able to directly insert and translocate across the lipid bilayer.[50–52] The influence on the energetics of the TSE by the 104–106 region, 120–122 region, and Met67, indicates that they may contribute a functional role in the unusual secretion mechanism of FGF-1. In this regard, we postulate that the SYM6ΔΔ mutant *in vivo* may exhibit an impaired ability to translocate across lipid bilayers and, therefore, might not be secreted if expressed within cells. The results also highlight the influence that specific turn regions can exert upon the TSE energetics and, therefore, the overall folding and unfolding kinetics of a protein.[53]

The SYM5 mutant was originally constructed to test the hypothesis that the core of a symmetric superfold could be effectively redesigned with a symmetric primary structure constraint.[18,19] This

design goal achieved a measure of success, but reached an apparent impasse when attempting to mutate a highly conserved Met at position 67. The solution to this impasse was postulated to require adjustments to the tertiary structure, involving deletions of two apparent structural insertions. Thus, the goal of increasing the primary structure symmetry appeared to be linked to a concomitant increase in the tertiary structure symmetry. The deletion of regions 104–106 and 120–122 has eliminated the structural requirement of Met at position 67, and an Ile mutation at this position can now be accommodated. Thus, the core region in the SYM6ΔΔ mutant is comprised of a total of four triplets of identical residue positions related by the 3-fold structural symmetry: Leu at positions 23, 65, and 109; Ile at positions 25, 67 and 111; Val at positions 31, 73, and 117; and Phe at positions 44, 85, and 132. There remains a single triplet region within the core to constrain to 3-fold symmetry, involving residues Leu14, Ile56 and Tyr97. In deleting these loop regions we have also increased the tertiary structure symmetry of FGF-1. In the FGF-1 structure each trefoil subdomain is a different length. The combined loop deletion (i.e. ΔΔ) mutants result in trefoil subdomains 2 and 3 being exactly 41 amino acid residues in length, while the first domain remains 42 amino acid residues in length (ignoring the details of the flexible amino terminus residues). Thus, there remains a modification of the first trefoil domain to produce a completely symmetric tertiary structure. In addition to the above-described core positions constrained to 3-fold symmetry, the substitution of the two Gly residues at positions 103 and 119 results in the symmetry-related residues at positions 20, 62 and 103, and 33, 75 and 119, being constrained to the same residue (Gly). Therefore, while WT* FGF-1 exhibits only a single triplet (positions 29, 71, and 115) with identical residues (Gly), the SYM6ΔΔ mutant has six additional positions. As noted, this symmetric-constraint redesign of FGF-1 has been accomplished with an ∼16 kJ/mol increase in stability in comparison to WT*. Although this increase in stability was unexpected, it has led us to propose the hypothesis that a primary structure symmetric constraint, within a symmetric protein superfold, might represent a solution to, rather than constraint upon, the stability and foldability of the polypeptide. We are pursuing additional core and turn mutations to increase the primary and tertiary structure symmetry of FGF-1 to test this hypothesis further.

Materials and Methods

Design of mutations

A prior structural and mutational analysis of a conserved Met residue at position 67 in FGF-1 indicated that it was intolerant of substitution and also resided within a unique packing environment that was not

conserved at the 3-fold symmetry-related positions of Ile25 and Leu111.[19] The local packing environment of Met67 includes two regions of apparent insertions, involving residue positions 104–106 and 120–122, in comparison to the symmetry-related positions (Figures 1 and 2). Deletion of these insertions was postulated to be a structural precondition to permit successful mutation of the Met67 residue. However, deletion was also postulated to result in the formation of adjacent β-turn structures, with a requirement of a Gly residue at positions 103[26] and 119, respectively (see Discussion for additional details). The 104–106 deletion in the present study thus includes an Ala103→Gly substitution mutation, and the 120–122 deletion mutation includes an Arg119→Gly substitution mutation. For brevity, the nomenclature for these deletion mutations is simply Δ104–106, and Δ120–122, respectively (Table 1). The combination of both deletion mutations is referred to as the ΔΔ mutation. The SYM5 and SYM6 core mutations have previously been described, and are designed to constrain the primary structure symmetry within the core to reflect the 3-fold tertiary structure symmetry.[19] The SYM5 mutant contains a total of five such core mutations, and the SYM6 mutant contains six (Table 1). The Δ104–106, Δ120–122, and ΔΔ mutations were constructed within the background of both the SYM5 and SYM6 core mutations.

Mutagenesis and expression

All studies utilized a synthetic gene for the 140 amino acid residue form of human FGF-1[54–56] with the addition of an amino-terminal six residue His-tag to facilitate purification using nickel nitrilotriacetic acid (Ni-NTA) affinity resin (QIAGEN, Valencia CA).[18] The Quik-Change™ site-directed mutagenesis protocol (Stratagene, La Jolla CA) was used to introduce mutations, individually or in combination, using mutagenic oligonucleotides of 25–31 bases in length (Biomolecular Analysis Synthesis and Sequencing Laboratory, Florida State University). For deletions involving residues 104–106 and 120–122, mutagenic oligonucleotides were used to delete these positions as well as simultaneously create point mutations Ala103→Gly and Arg119→Gly, respectively. For the construction of the combination deletion mutants, the Δ104–106 mutation was introduced into the Δ120–122 mutant background (in either SYM5 or SYM6 parental constructs). All FGF-1 mutants were expressed using the pET21a(+) plasmid/BL21(DE3) *Escherichia coli* host expression system (Invitrogen Corp., Carlsbad CA). Mutant construction, expression and purification followed previously described procedures.[18,27,57] Proteins containing the Δ120–122 mutation required substitution of Sephadex G-50 size-exclusion gel chromatography for the normally employed heparin Sepharose affinity chromatography step, since this mutation was deficient in heparin-binding functionality (see Results and Discussion).

Isothermal equilibrium denaturation

Protein samples were equilibrated overnight in 20 mM *N*-2-(acetamido)iminodiacetic acid (ADA), 100 mM NaCl (pH 6.60) at 298 K in 0.1 M increments of guanidine HCl (GuHCl). All samples contained a final protein concentration of 25 μM. An Aviv model 202 circular dichroism spectrometer (Proterion Corp., Piscataway, NJ) equipped with a Peltier-controlled temperature unit maintaining a constant temperature of 298 K was used for all spectroscopic measurements. For each sample, triplicate scans

were collected and averaged. Buffer traces were collected, averaged and subtracted from the sample traces. Data smoothing was performed prior to buffer subtraction using a five-point Fourier transform filter. The denaturation process was monitored by observing the change in CD signal at 227 nm with increasing GuHCl.[27] The general purpose non-linear, least-squares fitting program DataFit (Oakdale Engineering, Oakdale, PA) was used to fit the change in molar ellipticity at 227 nm *versus* GuHCl concentration to a six-parameter two-state model:[58]

$$F = (F_{0N} + S_N[D] + F_{0D} + S_D[D])$$
$$e^{-((\Delta G0 + m[D])/RT)}/1 + e^{-((\Delta G0 + m[D])/RT)} \quad (1)$$

where [D] is the denaturant concentration, F_{0N} and F_{0D} are the 0 M denaturant molar ellipticity intercepts for the native and denatured states, respectively, and S_N and S_D are the slopes of the native and denatured state baselines, respectively. ΔG_0 and m describe the linear function of the unfolding free energy *versus* denaturant concentration at 298 K. The effect of a given mutation upon the stability of the protein ($\Delta \Delta G$) was calculated by taking the difference between the C_m values for WT* and mutant, and multiplying by the average of the m values, as described by Pace and Scholtz:[59]

$$\Delta \Delta G = (C_{m\ WT*} - C_{m\ mutant})(m_{WT*} + m_{mutant})/2 \quad (2)$$

Folding kinetics measurements

Due to signal-to-noise considerations, relatively high protein concentrations ($>100\ \mu M$) of FGF-1 were required for kinetic studies monitored by CD. At these concentrations protein precipitation occurred in ADA buffer. Therefore, a different buffering system was chosen for the kinetic studies to permit higher protein concentrations without precipitation. Protein samples were dialyzed against 50 mM sodium phosphate, 100 mM NaCl, 10 mM ammonium sulfate, 2 mM DTT, and typically 2.5, 3.0 or 3.8 M GuHCl (pH 7.5) overnight at 298 K prior to data collection (higher concentrations of GuHCl were required to ensure complete denaturation for some stabilizing mutations). Protein samples were degassed for ten minutes prior to analysis. Refolding was initiated by a 1:10 dilution of protein solutions into 50 mM sodium phosphate, 100 mM NaCl, 10 mM ammonium sulfate, 2 mM DTT (pH 7.5) containing either 0.1 M or 0.05 M increments of GuHCl up to the midpoint of denaturation. All data were collected using an Aviv model SF305 stopped-flow system. Data collection times for each protein were designed to quantify the CD signal over five half-lives, or $>96\%$ of the total expected amplitude.

Unfolding kinetics measurements

Protein samples (300 μM) were dialyzed against 50 mM sodium phosphate, 100 mM NaCl, 10 mM ammonium sulfate, 2 mM DTT (pH 7.50) buffer overnight at 298 K, and degassed for ten minutes prior to data collection. Unfolding was initiated by 1:10 dilution of the native protein into 50 mM sodium phosphate, 100 mM NaCl, 10 mM ammonium sulfate, 2 mM DTT (pH 7.5) buffer with final GuHCl concentration in the range of 1.5–5.5 M in 0.5 M increments. The unfolding process was quantified by following the change in CD signal at 227 nm, and data collection times for each protein were designed so as

to monitor the CD signal over three to four half-lives, or >93% of the total expected amplitude.

Folding and unfolding kinetics analysis

Triplicate scans were collected for both folding and unfolding kinetic data at each GuHCl buffer condition. In all cases, data from at least three separate experiments were averaged. The kinetic rates and amplitudes *versus* denaturant concentration were calculated from the time-dependent change in CD signal using a single-exponential model:

$$I(t) = A\exp(-kt) + C \qquad (3)$$

where $I(t)$ is the intensity of CD signal at time t, A is the corresponding amplitude, k is the observed rate constant for the reaction and C is a constant that is the asymptote of the CD signal. Folding and unfolding rate constant data were fit to a global function describing the contribution of both rate constants to the observed kinetics as a function of denaturant (chevron plot):[45]

$$\ln(k_{obs}) = \ln(k_{f0}\exp(m_{kf}D) + k_{u0}\exp(m_{ku}D)) \qquad (4)$$

where k_{f0} and k_{u0} are the folding and unfolding rate constants, respectively, extrapolated to 0 M denaturant, m_{kf} and m_{ku} are the slopes of the linear functions relating $\ln(k_f)$ and $\ln(k_u)$, respectively, to D, the denaturant concentration. Changes in activation barriers upon mutation were calculated using a modified version of transition state theory:[60]

$$\Delta\Delta G_{\ddagger-D} = RT\ln(k_{f\ Mut}/k_{f\ WT*}) \text{ and } \Delta\Delta G_{\ddagger-N}$$

$$= RT\ln(k_{u\ Mut}/k_{u\ WT*}) \qquad (5)$$

where $k_{f\ Mut}$, $k_{u\ Mut}$, $k_{f\ WT^*}$ and $k_{u\ WT^*}$ are the folding and unfolding rates for mutant and WT*, respectively, in water. $\Delta\Delta G_{\ddagger-D}$ and $\Delta\Delta G_{\ddagger-N}$ are the changes in the activation barrier for folding and unfolding, respectively, between mutation and WT*. A positive value for $\Delta\Delta G_{\ddagger-D}$ or $\Delta\Delta G_{\ddagger-N}$ indicates a decrease in the associated activation barrier energy.

Isothermal titration calorimetry

All ITC data were collected on a VP-ITC microcalorimeter (MicroCal LLC, Northampton, MA). Titrations were performed at 298 K and all samples were equilibrated in 20 mM ADA, 100 mM NaCl (pH 6.60) buffer. All samples were filtered and degassed for ten minutes prior to loading. For WT* and SYM6/$\Delta\Delta$, 20 μM and 47 μM protein concentrations were used with sucrose octasulfate concentrations of 400 μM and 930 μM, respectively. The samples were titrated against 40 injections, at 4 μl per injection, of sucrose octasulfate. Each injection was performed over an eight seconds time-frame, with a post-injection equilibration period of 300 seconds. The titration curves were fit using the manufacturer's software (MicroCal Origin) employing a model with a single ligand-binding site.

Cell proliferation assay

NIH 3T3 fibroblasts were initially plated in Dulbecco's modified Eagle's medium (DMEM) (American Type Culture Collection, Manassas, VA) supplemented with 10% (v/v) newborn calf serum (NCS) (Sigma, St Louis, MO), 100 units of penicillin, 100 μg of streptomycin, 0.25 μg of Fungizone™ and 0.01 mg/ml of gentamicin (Gibco, Carlsbad CA) ("serum-rich" medium) in T75 tissue culture flasks (Fisher, Pittsburgh PA). The cultures were incubated at 37 °C and all cell growth was performed with 5% CO_2 supplementation. At 80% cell confluence, the cells were washed with 5 ml of cold TBS (0.14 M NaCl, 5.1 mM KCl, 0.7 mM Na_2HPO_4, 24.8 mM Trizma® base, pH 7.4) and subsequently treated with 5 ml of a 0.025% trypsin solution (Invitrogen Corp., Carlsbad CA). Cell synchronization was initiated by serum starvation in DMEM with 0.5% NCS, 100 units of penicillin, 100 μg of streptomycin, 0.25 μg of Fungizone™ and 0.01 mg/ml of gentamicin ("starvation" medium). The cells were seeded in T25 tissue culture flasks (Fisher, Pittsburgh, PA) at a cell density of 3.0×10^4 cells/cm^2 (representing ∼20% confluence). Duplicate flasks were used for each protein concentration. Cultures were incubated for 48 hours at 37 °C, the medium was then decanted and replaced with fresh medium supplemented with the appropriate concentration of FGF-1 protein, and incubated for an additional 48 hours. After this incubation, the medium was decanted and the cells were washed with 1 ml of cold TBS (pH 7.4). 1 ml of 0.025% trypsin was then added to release the cells from the flask surface, and 2 ml of serum-rich medium were added to dilute and inhibit the trypsin. The cells was counted using a hemacytometer (Hausser Scientific Partnership, Horsham, PA). Experiments were performed in quadruplicate and the cell densities were averaged. The relationship between the cell number and log concentration of added growth factor was fit to a sigmoidal function.

References

1. Orengo, C. A., Jones, D. T. & Thornton, J. M. (1994). Protein superfamilies and domain superfolds. *Nature*, **372**, 631–634.
2. Thornton, J. M., Orengo, C. A., Todd, A. E. & Pearl, F. M. (1999). Protein folds, functions and evolution. *J. Mol. Biol.* **293**, 333–342.
3. Schreiber, G., Buckle, A. M. & Fersht, A. R. (1994). Stability and function: two constraints in the evolution of barstar and other proteins. *Structure*, **2**, 945–951.
4. Shoichet, B. K., Baase, W. A., Kuroki, R. & Matthews, B. W. (1995). A relationship between protein stability and protein function. *Proc. Natl Acad. Sci. USA*, **92**, 452–456.
5. Wang, X., Minasov, G. & Shoichet, B. K. (2002).

Evolution of an antibiotic resistance enzyme constrained by stability and activity trade-offs. *J. Mol. Biol.* **320**, 85–95.

6. Bloom, J. D., Wilke, C. O., Arnold, F. H. & Adami, C. (2004). Stability and the evolvability of function in a model protein. *Biophys. J.* **86**, 2758–2764.

7. Tang, J., James, M. N., Hsu, I. N., Jenkins, J. A. & Blundell, T. L. (1978). Structural evidence for gene duplication in the evolution of the acid proteases. *Nature*, **271**, 618–621.

8. Holm, I., Ollo, R., Panthier, J. J. & Rougeon, F. (1984). Evolution of aspartyl proteases by gene duplication: the mouse renin gene is organized in two homologous clusters of four exons. *EMBO J.* **3**, 557–562.

9. Volbeda, A. & Hol, W. G. (1989). Pseudo 2-fold symmetry in the copper-binding domain of arthropodan haemocyanins. Possible implications for the evolution of oxygen transport proteins. *J. Mol. Biol.* **206**, 531–546.

10. Bergdoll, M., Eltis, L. D., Cameron, A. D., Dumas, P. & Bolin, J. T. (1998). All in the family: structural and evolutionary relationships among three modular proteins with diverse functions and variable assembly. *Protein Sci.* **7**, 1661–1670.

11. Lang, D., Thoma, R., Henn-Sax, M., Sterner, R. & Wilmanns, M. (2000). Structural evidence for evolution of the beta/alpha barrel scaffold by gene duplication and fusion. *Science*, **289**, 1546–1550.

12. Mukhopadhyay, D. (2000). The molecular evolutionary history of a winged bean α-chymotrypsin inhibitor and modeling of its mutations through structural analysis. *J. Mol. Evol.* **50**, 214–223.

13. Ponting, C. P. & Russell, R. B. (2000). Identification of distant homologues of fibroblast growth factors suggests a common ancestor for all beta-trefoil proteins. *J. Mol. Biol.* **302**, 1041–1047.

14. McLachlan, A. D. (1979). Three-fold structural pattern in the soybean trypsin inhibitor (Kunitz). *J. Mol. Biol.* **133**, 557–563.

15. Zhu, X., Komiya, H., Chirino, A., Faham, S., Fox, G. M., Arakawa, T. *et al.* (1991). Three-dimensional structures of acidic and basic fibroblast growth factors. *Science*, **251**, 90–93.

16. Murzin, A. G., Lesk, A. M. & Chothia, C. (1992). α-Trefoil fold. Patterns of structure and sequence in the kunitz inhibitors interleukins-1β and 1α and fibroblast growth factors. *J. Mol. Biol.* **223**, 531–543.

17. Blaber, M., DiSalvo, J. & Thomas, K. A. (1996). X-ray crystal structure of human acidic fibroblast growth factor. *Biochemistry*, **35**, 2086–2094.

18. Brych, S. R., Blaber, S. I., Logan, T. M. & Blaber, M. (2001). Structure and stability effects of mutations designed to increase the primary sequence symmetry within the core region of a β-trefoil. *Protein Sci.* **10**, 2587–2599.

19. Brych, S. R., Kim, J., Logan, T. M. & Blaber, M. (2003). Accommodation of a highly symmetric core within a symmetric protein superfold. *Protein Sci.* **12**, 2704–2718.

20. Springer, B. A., Pantoliano, M. W., Barbera, F. A., Gunyuzlu, P. L., Thompson, L. D., Herblin, W. F. *et al.* (1994). Identification and concerted function of two receptor binding surfaces on basic fibroblast growth factor required for mitogenesis. *J. Biol. Chem.* **269**, 26879–26884.

21. Pellegrini, L., Burke, D. F., von Delft, F., Mulloy, B. & Blundell, T. L. (2000). Crystal structure of fibroblast growth factor receptor ectodomain bound to ligand and heparin. *Nature*, **407**, 1029–1034.

22. Lobb, R. R. & Fett, J. W. (1984). Purification of two distinct growth factors from bovine neural tissue by heparin affinity chromatography. *Biochemistry*, **23**, 6295–6299.

23. Gospodarowicz, D., Cheng, J., Lui, G.-M., Baird, A. & Bohlen, P. (1984). Isolation by heparin-sepharose affinity chromatography of brain fibroblast growth factor: Identity with pituitary fibroblast growth factor. *Proc. Natl Acad. Sci. USA*, **81**, 6963–6967.

24. Zazo, M., Lozano, R. M., Ortega, S., Varela, J., Diaz-Orejas, R., Ramirez, J. M. & Gimenez-Gallego, G. (1992). High-level synthesis in *Escherichia coli* of a shortened and full-length human acidic fibroblast growth factor and purification in a form stable in aqueous solutions. *Gene*, **113**, 231–238.

25. Tsai, P. K., Volkin, D. B., Dabora, J. M., Thompson, K. C., Bruner, M. W., Gress, J. O. *et al.* (1993). Formulation design of acidic fibroblast growth factor. *Pharm. Res.* **10**, 649–659.

26. Kim, J., Brych, S. R., Lee, J., Logan, T. M. & Blaber, M. (2003). Identification of a key structural element for protein folding within β-hairpin turns. *J. Mol. Biol.* **328**, 951–961.

27. Blaber, S. I., Culajay, J. F., Khurana, A. & Blaber, M. (1999). Reversible thermal denaturation of human FGF-1 induced by low concentrations of guanidine hydrochloride. *Biophys. J.* **77**, 470–477.

28. Copeland, R. A., Ji, H., Halfpenny, A. J., Williams, R. W., Thompson, K. C., Herber, W. K. *et al.* (1991). The structure of human acidic fibroblast growth factor and its interaction with heparin. *Arch. Biochem. Biophys.* **289**, 53–61.

29. Zhu, X., Hsu, B. T. & Rees, D. C. (1993). Structural studies of the binding of the anti-ulcer drug sucrose octasulfate to acidic fibroblast growth factor. *Structure*, **1**, 27–34.

30. Volkin, D. B., Verticelli, A. M., Marfia, K. E., Burke, C. J., Mach, H. & Middaugh, C. R. (1993). Sucralfate and soluble sucrose octasulfate bind and stabilize acidic fibroblast growth factor. *Biochim. Biophys. Acta*, **1203**, 18–26.

31. Arunkumar, A. I., Kumar, T. K. S., Kathir, K. M., Srisailam, S., Wang, H. M., Leena, P. S. T. *et al.* (2002). Oligomerization of acidic fibroblast growth factor is not a prerequisite for its cell proliferation activity. *Protein Sci.* **11**, 1050–1061.

32. Spivak-Kroizman, T., Lemmon, M. A., Dikic, I., Ladbury, J. E., Pinchasi, D., Huang, J. *et al.* (1994). Heparin-induced oligomerization of FGF molecules is responsible for FGF receptor dimerization, activation and cell proliferation. *Cell*, **79**, 1015–1024.

33. Serrano, L., Horovitz, A., Avron, B., Bycroft, M. & Fersht, A. R. (1990). Estimating the contribution of engineered surface electrostatic interactions to protein stability by using double-mutant cycles. *Biochemistry*, **29**, 9343–9352.

34. Nagi, A. D. & Regan, L. (1997). An inverse correlation between loop length and stability in a four-helix-bundle protein. *Fold. Des.* **2**, 67–75.

35. Yayon, A., Klagsbrun, M., Esko, J. D., Leder, P. & Ornitz, D. M. (1991). Cell surface, heparin-like molecules are required for binding of basic fibroblast growth factor to its high affinity receptor. *Cell*, **64**, 841–848.

36. Pantoliano, M. W., Horlick, R. A., Springer, B. A., Van Dyk, D. E., Tobery, T., Wetmore, D. R. *et al.* (1994). Multivalent ligand-receptor binding interactions

in the fibroblast growth factor system produce a cooperative growth factor and heparin mechanism for receptor dimerization. *Biochemistry*, **33**, 10229–10248.

37. DiGabriele, A. D., Lax, I., Chen, D. I., Svahn, C. M., Jaye, M., Schlessinger, J. & Hendrickson, W. A. (1998). Structure of a heparin-linked biologically active dimer of fibroblast growth factor. *Nature*, **393**, 812–817.

38. McKeehan, W. L., Wu, X. & Kan, M. (1999). Requirement for anticoagulant heparan sulfate in the fibroblast growth factor receptor complex. *J. Biol. Chem.* **274**, 21511–21514.

39. Schlessinger, J., Plotnikov, A. N., Ibrahimi, O. A., Eliseenkova, A. V., Yeh, B. K. & Yayon, A. (2000). Crystal structure of a ternary FGF-FGFR-heparin complex reveals a dual role for heparin in FGFR binding and dimerization. *Mol. Cell Biol.* **6**, 743–750.

40. Hecht, H. J., Adar, R., Hofmann, B., Bogin, O., Weich, H. & Yayon, A. (2001). Structure of fibroblast growth factor 9 shows a symmetric dimer with unique receptor- and heparin-binding interfaces. *Acta Crystallog. sect. D*, **57**, 378–384.

41. Presta, M., Maier, J. A., Rusnati, M. & Ragnotti, G. (1989). Basic fibroblast growth factor is released from the endothelial extracellular matrix in a biologically active form. *J. Cell. Physiol.* **140**, 68–74.

42. Mach, H., Volkin, D. B., Burke, C. J., Middaugh, C. R., Linhardt, R. J., Fromm, J. R. *et al.* (1993). Nature of the interaction of heparin with acidic fibroblast growth factor. *Biochemistry*, **32**, 5480–5489.

43. Foresten, K. E., Courant, N. A. & Nugent, M. A. (1997). Endothelial proteoglycans inhibit bFGF binding and mitogenesis. *J. Cell. Physiol.* **172**, 209–220.

44. Natke, B., Venkataraman, G., Nugent, M. A. & Sasisekharan, R. (1999). Heparinase treatment of bovine smooth muscle cells inhibits fibroblast growth factor-2 binding to fibroblast growth factor receptor but not FGF-2 mediated cellular proliferation. *Angiogenesis*, **3**, 249–257.

45. Fersht, A. R. (1999). *Kinetics of Protein Folding. Structure and Mechanism in Protein Science*, W.H. Freeman, New York.

46. Abraham, J. A., Mergia, A., Whang, J. L., Tumolo, A., Friedman, J., Hjerrild, K. A. *et al.* (1986). Nucleotide sequence of a bovine clone encoding the angiogenic protein, basic fibroblast growth factor. *Science*, **233**, 545–548.

47. Jaye, M., Howk, R., Burgess, W., Ricca, G. A., Chiu, I.-M., Ravera, M. W. *et al.* (1986). Human endothelial cell growth factor: cloning, nucleotide sequence, and chromosome localization. *Science*, **233**, 541–544.

48. Weiner, H. L. & Swain, J. L. (1989). Acidic fibroblast growth factor mRNA is expressed by cardiac myocytes in culture and the protein is localized to the extracellular matrix. *Proc. Natl Acad. Sci. USA*, **86**, 2683–2687.

49. Florkiewicz, R. Z., Majack, R. A., Buechler, R. D. & Florkiewicz, E. (1995). Quantitative export of FGF-2 occurs through and alternative, energy-dependent, non-ER/Golgi pathway. *J. Cell. Physiol.* **162**, 388–399.

50. Jackson, A., Friedman, S., Zhan, X., Engleka, K. A., Forough, R. & Maciag, T. (1992). Heat shock induces the release of fibroblast growth factor 1 from NIH 3T3 cells. *Proc. Natl Acad. Sci. USA*, **89**, 10691–10695.

51. Wiedlocha, A., Madshus, I. H., Mach, H., Middaugh, C. R. & Olsnes, S. (1992). Tight folding of acidic fibroblast growth factor prevents its translocation to the cytosol with diphtheria toxin as vector. *EMBO J.* **11**, 4835–4842.

52. Mach, H. & Middaugh, C. R. (1995). Interaction of partially structured states of acidic fibroblast growth factor with phospholipid membranes. *Biochemistry*, **34**, 9913–9920.

53. Nagi, A. D., Anderson, K. S. & Regan, L. (1999). Using loop length variants to dissect the folding pathway of a four-helix-bundle protein. *J. Mol. Biol.* **286**, 257–265.

54. Gimenez-Gallego, G., Conn, G., Hatcher, V. B. & Thomas, K. A. (1986). The complete amino acid sequence of human brain-derived acidic fibroblast growth factor. *Biochem. Biophys. Res. Commun.* **128**, 611–617.

55. Linemeyer, D. L., Menke, J. G., Kelly, L. J., Disalvo, J., Soderman, D., Schaeffer, M.-T. *et al.* (1990). Disulfide bonds are neither required, present, nor compatible with full activity of human recombinant acidic fibroblast growth factor. *Growth Factors*, **3**, 287–298.

56. Ortega, S., Schaeffer, M.-T., Soderman, D., DiSalvo, J., Linemeyer, D. L., Gimenez-Gallego, G. & Thomas, K. A. (1991). Conversion of cysteine to serine residues alters the activity, stability, and heparin dependence of acidic fibroblast growth factor. *J. Biol. Chem.* **266**, 5842–5846.

57. Culajay, J. F., Blaber, S. I., Khurana, A. & Blaber, M. (2000). Thermodynamic characterization of mutants of human fibroblast growth factor 1 with an increased physiological half-life. *Biochemistry*, **39**, 7153–7158.

58. Eftink, M. R. (1994). The use of fluorescence methods to monitor unfolding transitions in proteins. *Biophys. J.* **66**, 482–501.

59. Pace, C. N. & Scholtz, J. M. (1997). Measuring the conformational stability of a protein. In *Protein Structure: A Practical Approach* (Creighton, T. E., ed), pp. 299–321, Oxford University Press, Oxford.

60. Fersht, A. R. (1999). *Structure and Mechanism in Protein Science*, W.H. Freeman, New York.